Journal of Solid State Chemistry 183 (2010) 497–503

Contents lists available at ScienceDirect

Journal of Solid State Chemistry

journal homepage: www.elsevier.com/locate/jssc

Uniform Ln^{3+} (Eu^{3+}, Tb^{3+}) doped $NaLa(WO_4)_2$ nanocrystals: Synthesis, characterization, and optical properties

Jun Gu, Yongchun Zhu, Haibo Li, Xianwen Zhang, Yitai Qian *

Department of Chemistry, Hefei National Laboratory for Physical Sciences at Microscale, University of Science and Technology of China, Hefei, Anhui 230026, China

ARTICLE INFO

Article history:
Received 28 July 2009
Received in revised form
31 October 2009
Accepted 19 December 2009
Available online 4 January 2010

Keywords:
Alkali rare earth tungstate
Crystal growth
Phosphor
Photoluminescence

ABSTRACT

Uniform shuttle-like Ln^{3+} (Eu^{3+}, Tb^{3+}) doped $NaLa(WO_4)_2$ nanocrystals have been solvothermally synthesized, and the size of the nanocrystals could be easily controlled by adjusting the volume ratio of ethylene glycol (EG) to water. Doped with 5 mol% Eu^{3+} and Tb^{3+} ions, the $NaLa(WO_4)_2$ nanocrystals showed strong red and green emissions with lifetimes of 0.8 and 1.40 ms, respectively. A high quenching concentration of 15 mol% was observed in Eu^{3+}-doped $NaLa(WO_4)_2$ nanocrystals and 35 mol% in Tb^{3+}-doped $NaLa(WO_4)_2$ nanocrystals. The emission intensity measurements of Eu^{3+}-doped $NaLa(WO_4)_2$ with different sizes indicated that the emission intensity of shuttles with length of 300 nm in average was stronger than that of shuttles with length of 900 nm in average, but was weaker than that of needles with length of 4 and 9 μm in average.

1. Introduction

Alkali rare earth tungstates ($ARe(WO_4)_2$, where A=alkali metal ions, Re=rare earth ions) are of particular interest since they are good laser hosts [1,2], efficient Raman active medium [3], and have potential applications in quantum electronics [4], visual display [5], solid-state lighting [6], and fluorescence labels [7]. Sodium lanthanum tungstate $NaLa(WO_4)_2$ has the scheelite ($CaWO_4$) structure with a space group of $I_{41/a}$, and is a good host material for rare earth ions to design luminescent materials, which exhibits efficient photoluminescence properties due to an efficient energy transfer from tungstate groups to activator ions [8,9]. Rare earth (Eu^{3+}, Nd^{3+}, and Er^{3+}) doped $NaLa(WO_4)_2$ spherical powders with diameters of 1–2 μm synthesized by a hydrothermal method exhibited a higher quenching concentration of 25 mol% and a long lifetime of 1.02 ms [8]. Rare earth (Eu^{3+}, Yb^{3+}, and Er^{3+}) doped $NaLa(WO_4)_2$ irregular nanoparticles with an average size of 10∼30 nm were hydrothermally obtained with a subsequent heat treatment of 600 °C, which display strong upconversion luminescence [9].

Here, we reported the synthesis of uniform shuttle-like Ln^{3+} (Eu^{3+}, Tb^{3+}) doped $NaLa(WO_4)_2$ nanocrystals by a solvothermal route. The nanocrystals are 300 nm in length and 100 nm in width. The size and the aspect ratio of shuttles increased with the decrease of the volume ratio of EG to water. In addition, the lifetime of 5 mol% Eu^{3+} and Tb^{3+} ions doped $NaLa(WO_4)_2$ nanocrystals was 0.8 and 1.40 ms, respectively. Quenching concentration of 15 mol% was observed in Eu^{3+}-doped $NaLa(WO_4)_2$ nanocrystals and 35 mol% in Tb^{3+}-doped $NaLa(WO_4)_2$ nanocrystals. The emission intensity of Eu^{3+} doped $NaLa(WO_4)_2$ with different size were also investigated.

2. Experimental section

2.1. Synthesis of $NaLa(WO_4)_2$:Ln nanocrystals

All the reagents used in the experiment were analytical pure (purchased from Shanghai Chemical Industrial Co.) and used without further purification. In a typical experiment, 0.75 mmol of $La(NO_3)_3 \cdot 6H_2O$ (including $EuCl_3 \cdot 6H_2O$ or $TbCl_3 \cdot 6H_2O$) were dissolved in 45 mL mixture solution (5 mL distilled water and 40 mL EG) under vigorous stirring, and then 5 mL aqueous solution containing 2.0 mmol $Na_2WO_4 \cdot 6H_2O$ was added to above transparent solution with vigorous stirring continuously for about 20 min. A translucent solution (the volume ratio of V_{EG}: V_{water}=4:1) was obtained and transferred into a 60 mL Teflon-lined stainless autoclave. The autoclave was sealed and maintained at 180 °C for 16 h and then cooled to room-temperature naturally. The white precipitate was separated by centrifugation and washed with ethanol for several times, and then dried in a vacuum at 60 °C for 6 h.

2.2. Characterization

The X-ray power diffraction (XRD) pattern of the products was recorded on a Philips X'pert X-ray diffractometer equipped with

* Corresponding authors. Fax: +86 551 3607402.
E-mail addresses: ychzhu@ustc.edu.cn (Y. Zhu), ytqian@ustc.edu.cn (Y. Qian).

0022-4596/$ - see front matter © 2009 Elsevier Inc. All rights reserved.
doi:10.1016/j.jssc.2009.12.019

CuKα radiation (λ=1.54178 Å). The field emission scanning electron microscope (FESEM) images of the products were recorded on a JEOL-JSM-6700F field-emitting microscope. The morphologies of the products were observed with JEM-2010 transmission electron microscope (TEM) using an accelerating voltage of 200 kV with a tungsten filament. High-resolution transmission electron microscopy (HRTEM) images and selected area electron diffraction (SAED) patterns were obtained on JEOL-2010 transmission electron microscope at an accelerating voltage of 200 kV. The photoluminescence spectra and the luminescence decay curves of the samples were measured by a steady-state/lifetime spectrofluorometer (JOBIN YVON, FLUOROLOG-3-TAU) with a 450 W monochromatized xenon lamp.

3. Results and discussion

3.1. Morphology and structure of the products

A typical XRD pattern of the 5 mol% Eu^{3+}-doped products is shown in Fig. 1. All reflection peaks of the different product can be indexed to a tetragonal-phase $NaLa(WO_4)_2$ with calculated lattice constants of a=5.349 Å and c=11.62 Å, which are consistent with the standard values reported in JCPDS 79-1118, and no other impurity peaks were detected. It is worth noting that no crystal structure change of $NaLa(WO_4)_2$ was found after doping with Eu^{3+} or Tb^{3+} ions.

Representative FESEM and TEM images of the products, as shown in Fig. 2a and b, clearly display highly uniform monodisperse distribution shuttle-like nanocrystals with length of 300 nm in average and middle width of 100 nm in average. The high-magnification TEM image of an individual crystal (Fig. 2c) gives more details on the morphology of the nanocrystal. The HRTEM image (Fig. 2d) of the part in pane of Fig. 2c shows the interplanar spacing of 0.582 and 0.380 nm, which corresponds to the double lattice spacing for (004) plane and (110) plane of tetragonal-phase $NaLa(WO_4)_2$, respectively. The corresponding SEAD pattern along the [1$\bar{1}$0] zone axis shows that the diffraction dots can be indexed as the (002), (112) and (110) plane of tetragonal-phase $NaLa(WO_4)_2$, consistent with the results of HRTEM. Both the HRTEM image and the SAED pattern reveal that the as-prepared shuttle-like nanocrystals are single-crystalline and have a preferential [001] growth direction.

The growth process of Ln^{3+}-doped $NaLa(WO_4)_2$ shuttle-like nanocrystals was monitored by investigating the products obtained at different stages of the reaction using TEM and XRD techniques. Fig. 3a shows the XRD patterns of the products obtained at different reaction stages. As can be seen that there were no obvious

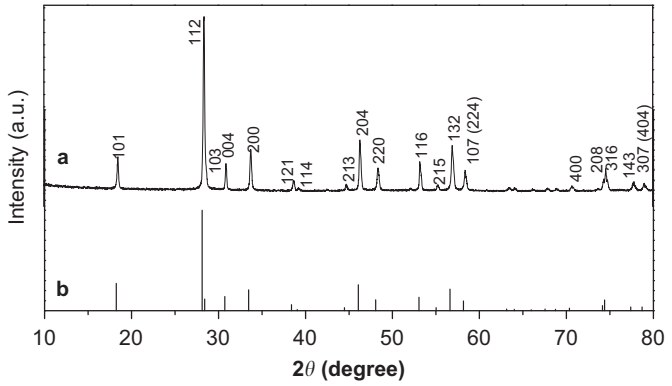

Fig. 1. (a) A typical XRD pattern of the products; (b) The standard card of JCPDS 79–1118.

tetragonal-phase $NaLa(WO_4)_2$ observed at the preliminary stage of reaction (20 and 40 min). As the aging time was prolonged to 60 min or longer, a single phase of tetragonal $NaLa(WO_4)_2$ formed, and the crystallinity of products became better with the aging time increasing. Fig. 3b–e presents the TEM images of products obtained at different reaction stages, which clearly show the transformation process from irregular aggregates to shuttle-like nanocrystals. After the reaction for 20 min, a white-translucent suspension was observed. Fig. 3b shows the typical TEM image of the products obtained after 20 min, which reveals the products were irregular aggregates. When the reaction time was increased to 40 min, only a few primary shuttle-like nanocrystals appeared (Fig. 3c). Then the reaction time was prolonged to 1 h, and a great quantity of shuttle-like nanocrystals formed (Fig. 3d). However, some irregular aggregates still existed in the products and the size of nanocrystals was not uniform. At last, uniform high quality shuttle-like nanocrystals were obtained with the aging time up to 2 h or longer, which is shown in Fig. 3e and 2b.

Fig. 4 shows the FT-IR spectrums of the products obtained at various reaction stages. The broad bands at ~3400 and ~1640 cm^{-1} correspond to the O–H stretching vibration and the O–H bending vibration, coming from physically absorbed water or EG [10]. The IR-absorption bands at ~2930 and ~2875 cm^{-1} can be attributed to the C–H stretching vibration. The peak at ~1080 cm^{-1} can be assigned to the C–O stretching vibration. The strong absorption bands at ~930, ~810, and ~419 cm^{-1} correspond to the υ1, υ3 and υ2 modes of the WO_4^{2-} groups in tungstate, respectively [11]. The characteristic bands of the WO_4^{2-} groups appeared when the aging time was more than 60 min, indicating that the $NaLa(WO_4)_2$ formed after 60 min.

To investigate the effect of the solvent for the size and morphology of the products, a series experiments with different volume ratio of EG to water were carried out keeping other synthetic parameters constant. Typical FESEM images of the products are shown in Fig. 5. When the ratio of V_{EG}:V_{water} was 4:1, shuttle-like nanocrystals with length of 300 nm in average and middle width of 100 nm in average (The aspect ratio of shuttle is about 3, as shown in Fig. 2a, b and 5a) were obtained. Decreasing the ratio of V_{EG}:V_{water} to 3:2, uniform shuttle-like microcrystals with length of 900 nm in average and middle width of 200 nm in average (The aspect ratio of shuttle is about 4.5, as shown in Fig. 5b) were obtained. Fig. 5 shows that uniform needle-like microcrystals with length of 4 μm in average and middle width of 500 nm in average (The aspect ratio of needle is about 8) were obtained when the ratio of V_{EG}:V_{water} was 2:3. When the ratio of V_{EG}:V_{water} decreased to 1:4, the average length and width of needle-like microcrystals was increased to 8–9 and 1 μm, respectively (The aspect ratio of needle is about 9, as shown in Fig. 5d). In addition, there were no tetragonal-phase $NaLa(WO_4)_2$ when the solvent was pure EG, and irregular massive tetragonal-phase $NaLa(WO_4)_2$ products were obtained when the solvent was water without EG. Obviously, the appropriate ratio of V_{EG}:V_{water} was crucial to the formation of uniform small-size nanocrystals, and the decreasing the volume ratio of EG to water led to a dramatic increase in the size of the products.

The above experimental results suggest that EG plays a key role in the growth process of nanocrystals for our synthetic process. It is well known that EG possesses good coordinating ability [12]. Similar to the formation of SnO_2, TiO_2, In_2O_3, PbO nanowires by a polyol process described in the work of Jiang et al. [13], EG serves as a ligand to form stable complexes with La^{3+}, which can be further testified by the phenomenon that no precipitates appeared with the Na_2WO_4 introduced into the transparent mixture solution containing La^{3+} ions, EG, and water. However, the coordination complex is not stable at 180 °C and can release La^{3+} and EG again. With the reaction proceeding

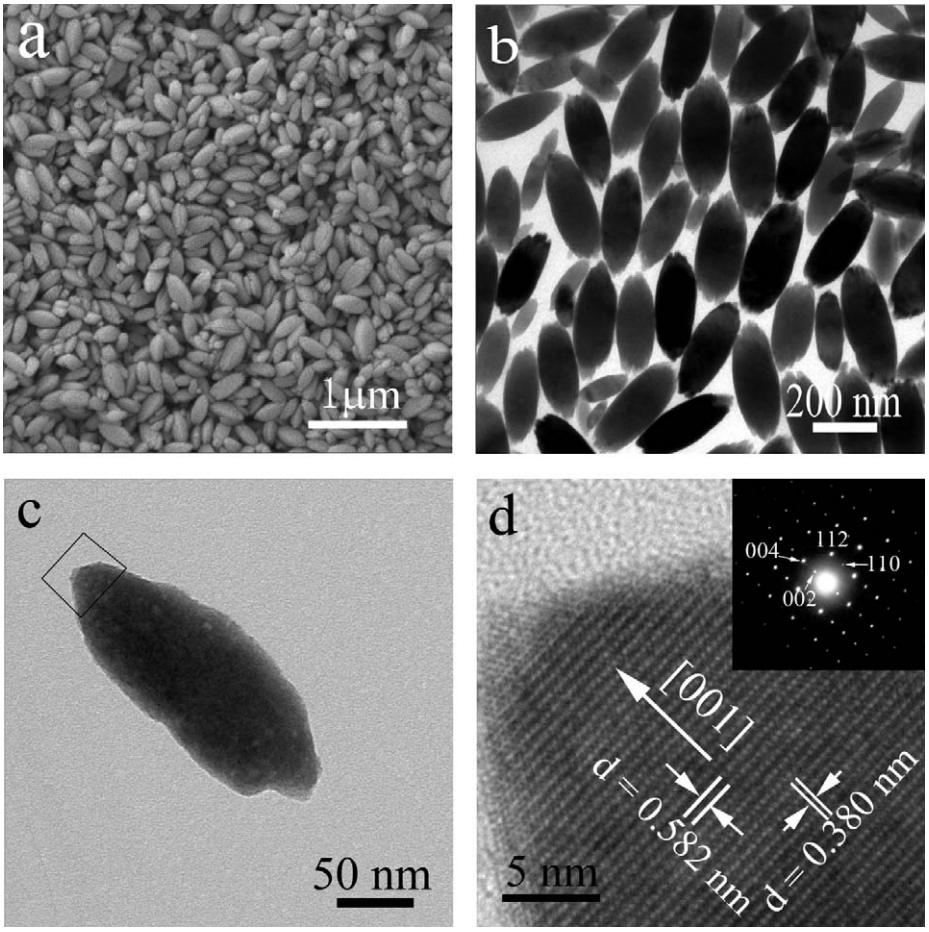

Fig. 2. (a, b) Typical FESEM and TEM images of the products, respectively; (c) high-magnification TEM image of an individual nanocrystal; (d) HRTEM image and the inserted SEAD pattern both recorded from the marked place by pane in Fig. 2c.

continuously, La^{3+} ions reacted with Na_2WO_4 to form $NaLa(WO_4)_2$ nanoparticles, which further self-assembled into shuttle-like nanocrystals. In the growth process of nanocrystals, EG can also selectively adsorb and stabilize some crystal plans, which causes the anisotropic growth of $NaLa(WO_4)_2$ nanocrystals. Similar role of EG has been reported in synthesis of metal sulfides in polyol media [14,15]. In addition, the size of products was increased with decrease of the volume ratio of EG to water in our synthetic process. It can be attributed to the special physical and chemical properties such as the viscosity and chelation for different concentration of EG, which can affect the solubility, diffusion and reactivity behavior of reactants and further affect the growing speed and the size of $NaLa(WO_4)_2$ crystals [16,17].

3.2. Optical properties

Room temperature photoluminescence (PL) spectra of the synthesized shuttle-like $NaLa(WO_4)_2$ nanocrystals doped with Ln^{3+} (Eu^{3+} and Tb^{3+}) were investigated. Fig. 6 shows the excitation and emission spectra of the 5 mol% Eu^{3+}-doped $NaLa(WO_4)_2$ nanocrystals prepared at 180 °C for 16 h. The excitation spectrum (Fig. 6I) monitored by the $^5D_0 \rightarrow {}^7F_2$ emission of Eu^{3+} (614 nm) contains a broadband ranging from 250 to 300 nm due to the charge transfer transition of O→W in WO_4^{2-} groups, which indicates the energy transfer from WO_4^{2-} to Eu^{3+} [18]. The *f–f* transition lines at ~361 nm ($^7F_0 \rightarrow {}^5D_4$), ~381 nm ($^7F_0 \rightarrow {}^5L_7$), ~393 nm ($^7F_0 \rightarrow {}^5L_6$), and ~464 nm ($^7F_0 \rightarrow {}^5D_2$) of Eu^{3+} have also been detected. Fig. 6II shows the emission spectra of products excited by 393 and 270 nm, respectively. The majority of the emission spectrum contains only the $^5D_0 \rightarrow {}^7F_J$ (J=0–4) transitions. The emission spectrum excited by 393 nm shows that the electric dipole transition $^5D_0 \rightarrow {}^7F_2$ (at 614 nm) is about six times stronger than the magnetic dipole transition $^5D_0 \rightarrow {}^7F_1$ (at 590 nm), which indicates that Eu^{3+} ions occupy noninversion center sites in Eu^{3+}-doped $NaLa(WO_4)_2$ nanocrystals [8,9]. The emission spectrum under 270 nm excitation includes a broadband (inset in Fig. 6II) and three narrow $^5D_0 \rightarrow {}^7F_J$ (J=1, 2, and 4) emission bands appearing at 590, 614, and 700 nm, respectively. The broadband range from 320 to 500 nm, peaking at 390 nm in the short wavelength region, originates from O→W charge transfer transition. Its weak intensity reveals that the energy transfer from WO_4^{2-} group to Eu^{3+} is complete.

The as-prepared $NaLa(WO_4)_2$ shuttle-like nanocrystals doped with Tb^{3+} ions display strong green luminescence. Fig. 7 shows the emission spectrum of the 5 mol% Tb^{3+}-doped $NaLa(WO_4)_2$ nanocrystals under the excitation of 270 nm. The splitting and the intensity pattern of the luminescence lines indicate the successful doping of Tb^{3+}. The emission mainly result from the transitions of the $^5D_4 \rightarrow {}^7F_J$ (J=6, 5, 4, 3) level, peaking at 488, 543, 583, and 621 nm, respectively. The strongest brightgreen emission at 543 nm corresponds to the $^5D_4 \rightarrow {}^7F_5$ transition.

Fig. 8 displays the luminescence decay curves of the $^5D_0 \rightarrow {}^7F_2$ emission (614 nm) of Eu^{3+} (I) and the $^5D_4 \rightarrow {}^7F_5$ emission (543 nm) of Tb^{3+} (II) in the 5 mol% Ln^{3+} (Eu^{3+}, Tb^{3+}) doped $NaLa(WO_4)_2$

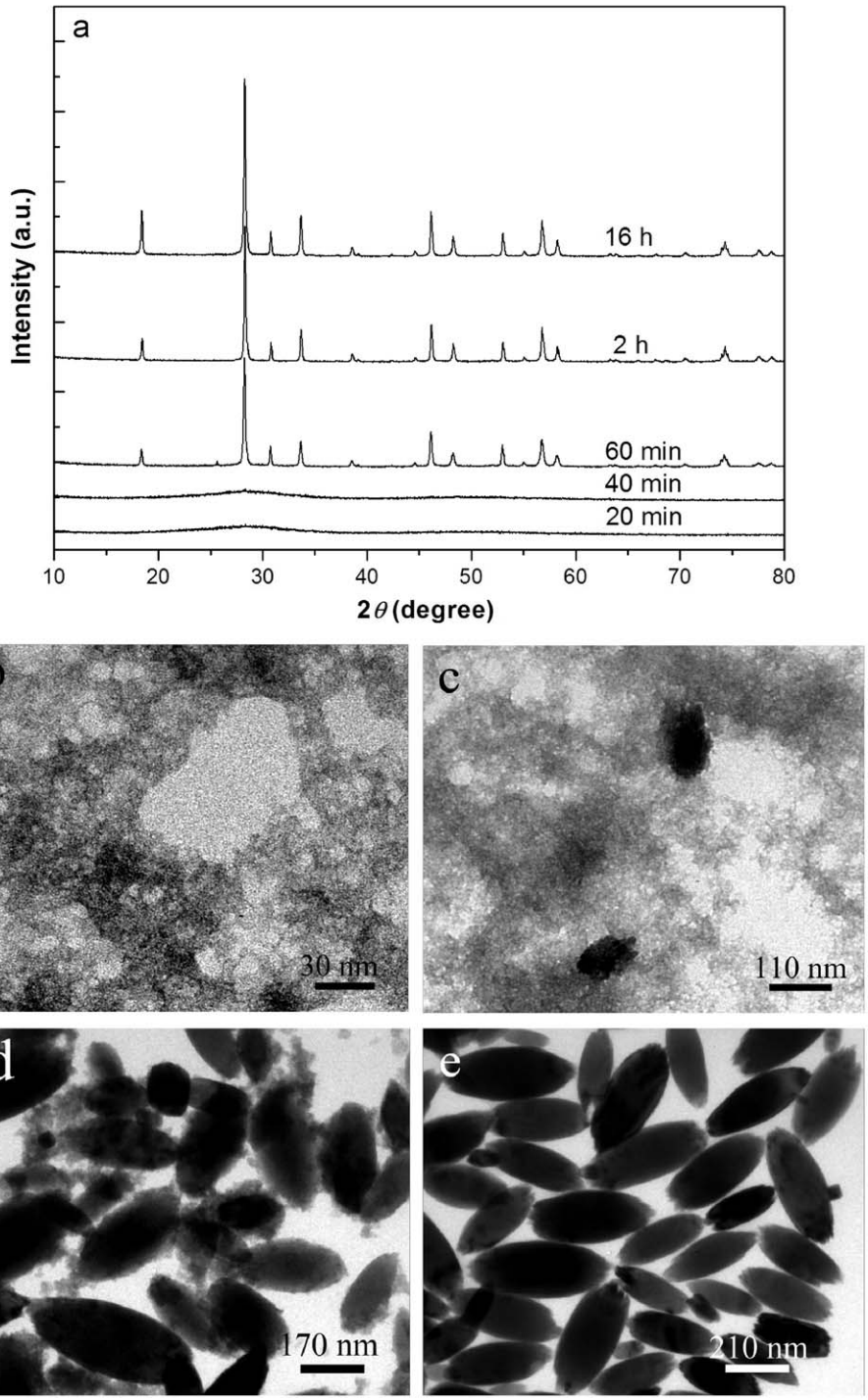

Fig. 3. (a) XRD patterns of the products obtained at various reaction stages and typical TEM images of the products obtained at various reaction stages: (b) 20 min; (c) 40 min; (d) 1 h; and (e) 2 h.

nanocrystals under λ_{ex}=270 nm. These decay curves can be well fitted into a single exponential function $I=I_0\exp(-t/\tau)$ (τ is the $1/e$ lifetime of the rare earth ion, I_0 is the initial intensity at $t=0$), from which we can give the lifetime of the $^5D_0\rightarrow{}^7F_2$ emission of Eu^{3+} τ=0.80 ms and the lifetime of the $^5D_4\rightarrow{}^7F_5$ emission of Tb^{3+} τ=1.40 ms.

It is well known that the emission intensity of phosphor is strongly dependent on the doping concentration of rare earth ions. Fig. 9I shows the relationship between the luminescence intensity of the Eu^{3+}-doped $NaLa(WO_4)_2$ nanocrystals by monitoring the emission of $^5D_0\rightarrow{}^7F_2$ transition and mole percent of Eu^{3+} ions. The luminescence intensity increases with the increase of doping concentration and reaches a maximum at 15 mol% Eu^{3+} doping concentration. The same tendency happens in that of Tb^{3+}-doped $NaLa(WO_4)_2$ nanocrystals. As described in Fig. 9II, the luminescence intensity of Tb^{3+}-doped $NaLa(WO_4)_2$ nanocrystals by monitoring the emission of $^5D_4\rightarrow{}^7F_5$ transition reaches a maximum at 35 mol% Tb^{3+} doping concentration, from which the higher concentration quenching can be displayed. Generally, the concentration quenching effect is associated with

the possible nonradiative transfer originating from resonance energy transfer between neighboring rare-earth ions, which increases the mobility of the excited state within the host matrix and the probability of nonradiative deexcitation via traps [19,20]. Quenching occurs easily in particles containing many traps when increasing the concentration of luminescent center. In nanomaterials, since only a few traps caused by the limited unit cells in per particle and the resonance energy transfer only occurs within one particle due to the hindrance by the particle boundary, quenching occurs at higher doped concentration [20]. Wang et al. have investigated the concentration quenching of the Eu^{3+}-doped $NaLa(WO_4)_2$ powers [8]. In $NaLa(WO_4)_2$ crystal, Ln^{3+} occupy the La^{3+} sites of LaO_8 polyhedrons which are isolated from each other and joined by means of La–O–W–O–La. It is disadvantageous to transfer energy between Ln^{3+} ions for this architecture. Therefore,

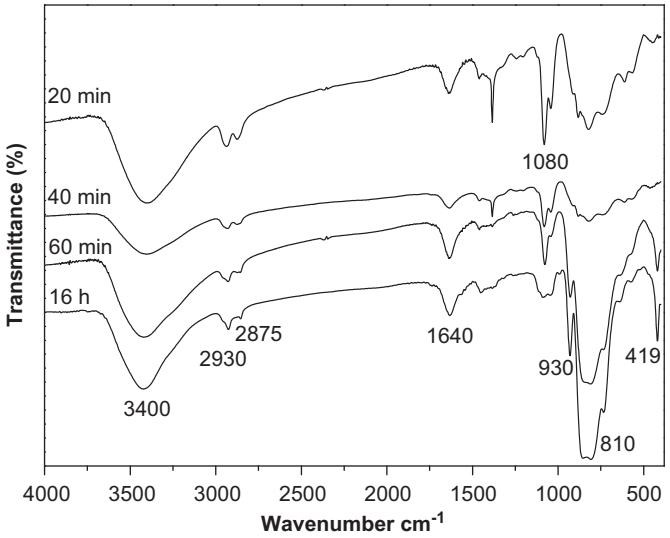

Fig. 4. FT-IR spectrums of the products obtained at different reaction stages.

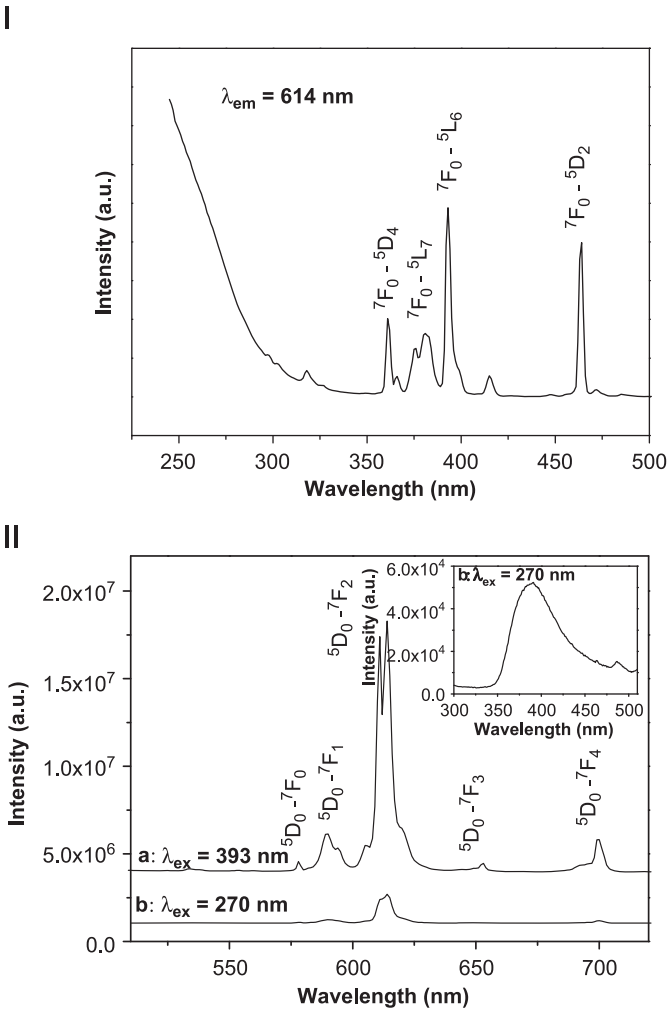

Fig. 6. Excitation (I) and emission (II) spectra of the 5 mol% Eu^{3+}-doped $NaLa(WO_4)_2$ nanocrystals.

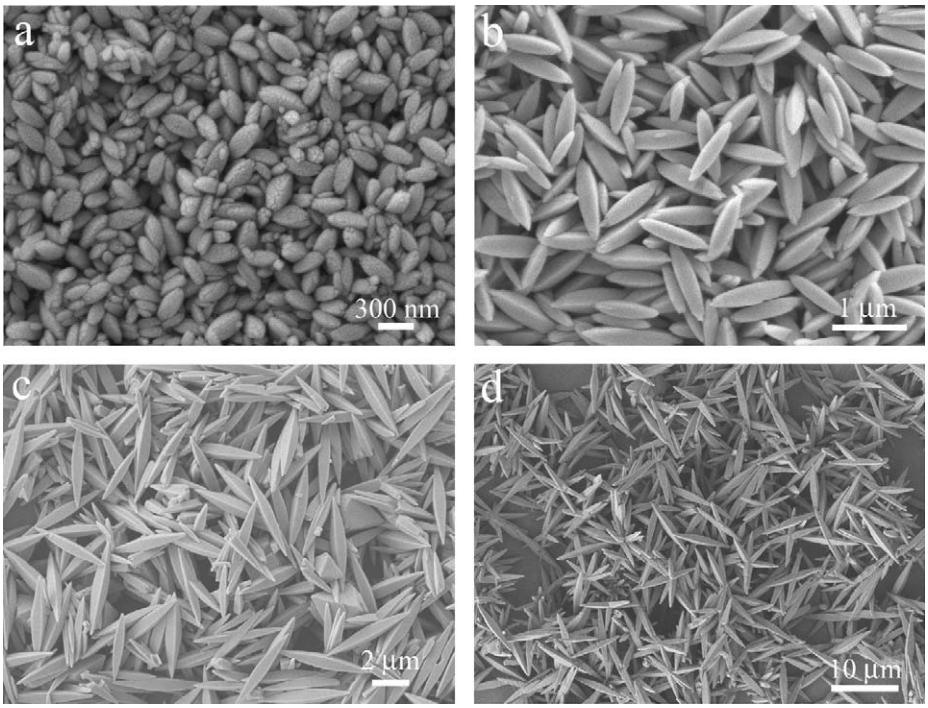

Fig. 5. Typical FESEM images of the products obtained at 180 °C for 16 h with different ratio of V_{EG}:V_{water}: (a) 4:1, (b) 3:2, (c) 2:3, and (d) 1:4.

higher concentration quenching was observed in our Ln^{3+}-doped $NaLa(WO_4)_2$ nanocrystals, which would be of great benefit to their practical uses.

The properties of inorganic nanomaterials are greatly affected by their morphology, size, and crystallinity. From above description, $NaLa(WO_4)_2$ crystals with different size were obtained by adjusting the ratio of V_{EG}:V_{water}. To investigate the influence of size and morphology on the optical property of the products, the emission intensity of Eu^{3+}-doped $NaLa(WO_4)_2$ crystals with different size was measured. Fig. 10I and II shows the emission spectra of different size 5 mol% Eu^{3+}-doped $NaLa(WO_4)_2$ nanocrystals excited at 393 and 270 nm, respectively, from which it can be seen that emission intensity of the products is remarkably influenced by their size, but the peak positions of the emission remain the same. It is obviously that whether monitored by 393 or 270 nm, the emission intensity of nanocrystals with an average length of 900 nm is weaker than that of nanocrystals with an average length of 300 nm, and then the emission intensity rapidly increases with length increasing from 900 to 9 μm. Fig. 10III shows the XRD pattern of these products. As can be seen, the crystallinity of the products increases with the size of products increasing. As we know, luminescence efficiency increases with the decreasing crystallite size [21], while high crystallinity always means less traps and stronger luminescence [22]. Here, the size effect is primary when the size of nanocrystals is <900 nm, and the effect of crystallinity for emission intensity is dominant when the crystallite size is more than 900 nm. So the result described in Fig. 10IV is reasonable. The size dependence of the fluorescence intensity can be demonstrated from the quantum confinement model as described by Bawendi et al. [23,24] or in terms of the amount of particles per unit area facing towards the incident light as described by Pramod et al [25].

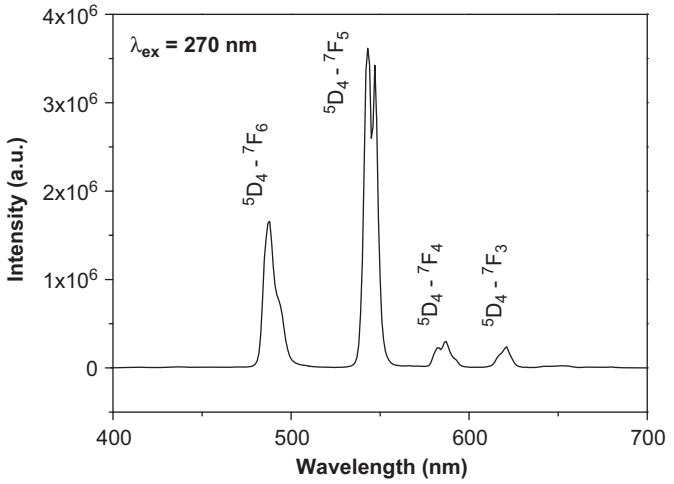

Fig. 7. Emission spectra of the 5 mol% Tb^{3+}-doped $NaLa(WO_4)_2$ nanocrystals.

4. Conclusion

In summary, uniform shuttle-like Ln^{3+} (Eu^{3+}, Tb^{3+}) doped $NaLa(WO_4)_2$ nanocrystals have been synthesized in a binary solution system made of ethylene glycol and distilled water. The growth process of shuttle-like nanocrystal and the effects of

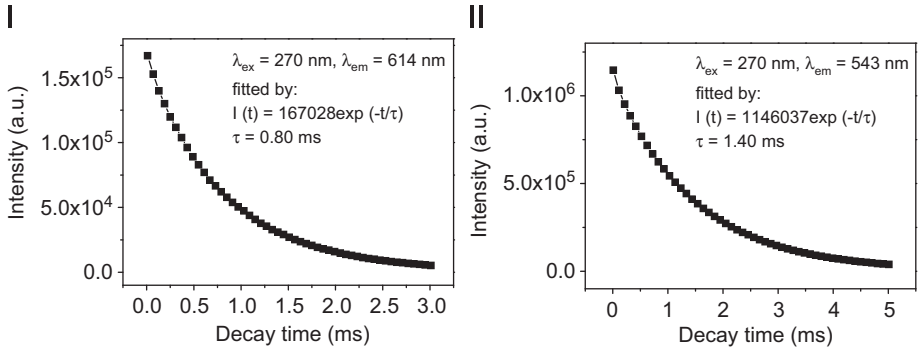

Fig. 8. Luminescence decay curves of (I) the 614 nm emission of Eu^{3+} ions and (II) 543 nm emission of Tb^{3+} in the 5 mol% Ln^{3+} (Eu^{3+}, Tb^{3+}) doped $NaLa(WO_4)_2$ nanocrystals under λ_{ex}=270 nm.

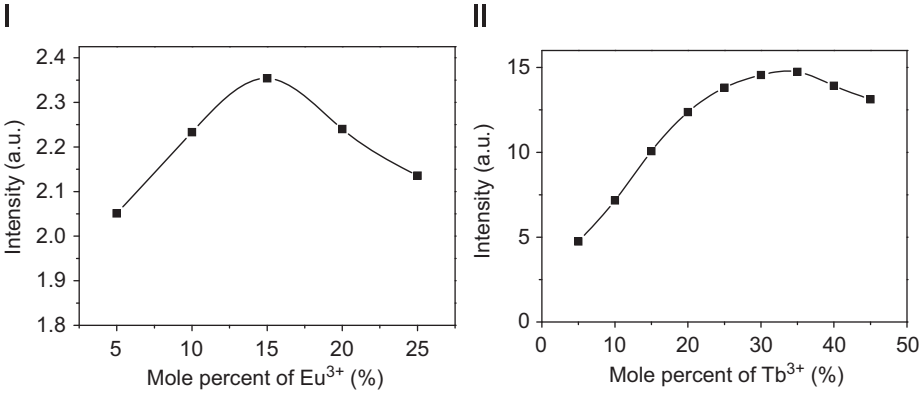

Fig. 9. Relationship between the luminescence intensity of the Ln^{3+}-doped $NaLa(WO_4)_2$ nanocrystals and mole percent of Ln^{3+} ions: (I) emission intensity centered at 614 nm ($^5D_0 \rightarrow {}^7F_2$) of Eu^{3+} under the excitation of 270 nm, (II) emission intensity centered at 543 nm ($^5D_4 \rightarrow {}^7F_5$) of Tb^{3+} under the excitation of 270 nm.

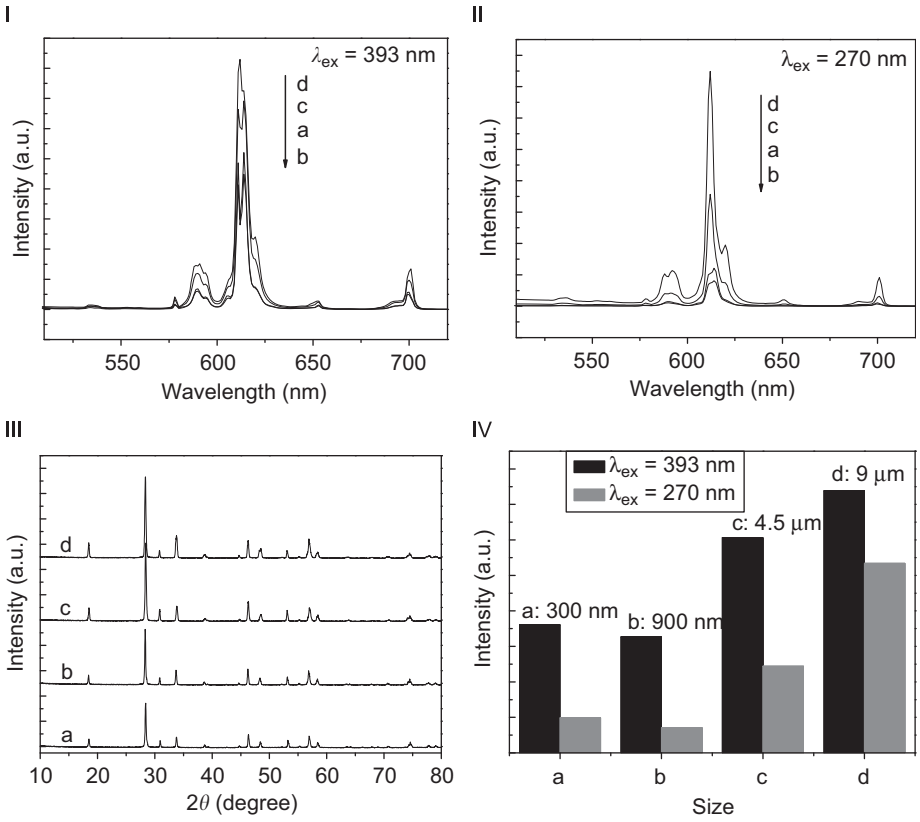

Fig. 10. (I, II) Emission spectra, (III) XRD pattern, and (IV) emission intensity centered at 614 nm of the 5 mol% Eu^{3+}-doped $NaLa(WO_4)_2$ crystals prepared at 180 °C for 16 h with different ratio of V_{EG}: V_{water}: (a) 4:1, (b) 3:2, (c) 2:3, and (d) 1:4.

the ratio of V_{EG}:V_{water} on the size of products were investigated. The Eu^{3+} and Tb^{3+}-doped $NaLa(WO_4)_2$ nanocrystals display strong red and green emission after excitation by ultraviolet light, respectively. The Ln^{3+} (Eu^{3+}, Tb^{3+}) doped $NaLa(WO_4)_2$ nanocrystals exhibit long lifetime and high quenching concentration. It is found that the size and crystallinity of products have great influence on their emission intensity.

Acknowledgment

The financial support of this work, by National Natural Science Foundation of China (no.20431020) and the 973 Project of China (no. 2005CB623601), is gratefully acknowledged.

References

[1] J. Liu, J.M. Cano-Torres, C. Cascales, F. Esteban-Betegón, M.D. Serrano, V. Volkov, C. Zaldo, M. Rico, U. Griebner, V. Petrov, Phys. Stat. Sol. (a) 4 (2005) R29.
[2] A. García-Cortés, C. Cascales, A.D. Andrés, C. Zaldo, E.V. Zharikov, K.A. Subbotin, S. Bjurshagen, V. Pasiskevicius, M. Rico, IEEE J. Quantum Elect. 43 (2007) 157.
[3] A.A. Kaminskii, S.N. Bagaev, D. Grebe, H.J. Eichler, A.A. Pavlyuk, R. Macdonald, Quantum Electron. 26 (1996) 193.
[4] A.A. Kaminskii, H.J. Eichler, K. Ueda, N.V. Klassen, B.S. Redkin, L.E. Li, J. Findeisen, D. Jaque, J. García-Sole, J. Fernández, R. Balda, Appl. Opt. 38 (1999) 4533.
[5] Y.R. Do, Y.D. Huh, J. Electrochem. Soc. 147 (2000) 4385.
[6] S. Neeraj, N. Kijima, A.K. Cheetham, Chem. Phys. Lett. 387 (2004) 2.
[7] N. Xue, X. Fan, Z. Wang, M. Wang, Mater. Lett. 61 (2007) 1576.
[8] F. Wang, X.P. Fan, D.B. Pi, Z.Y. Wang, M.Q. Wang, J. Solid State Chem. 178 (2005) 825.
[9] N. Xue, X.P. Fan, Z.Y. Wang, M.Q. Wang, J. Phys. Chem. Solids 69 (2008) 1891.
[10] X. Jiang, Y. Wang, T. Herricks, Y. Xia, J. Mater. Chem. 14 (2004) 695.
[11] S.P.S. Porto, J.F. Scott, Phys. Rev. 157 (1967) 716.
[12] O. Yamamoto, T. Sasamoto, M. Inagaki, J. Mater. Res. 7 (1992) 2488.
[13] X.C. Jiang, Y.L. Wang, T. Herricksb, Y.N. Xia, J. Mater. Chem. 14 (2004) 695.
[14] D. Chen, K. Tang, G. Shen, J. Sheng, Z. Fang, X. Liu, H. Zheng, Y. Qian, Mater. Chem. Phys. 82 (2003) 206.
[15] C. Feldmann, C. Metzmacher, J. Mater. Chem. 11 (2001) 2603.
[16] X. Zhang, Z. Ai, F. Jia, L. Zhang, J. Phys. Chem. C 112 (2008) 747.
[17] Y. Zhou, H. Yao, Q. Zhang, J. Gong, S. Liu, S. Yu, Inorg. Chem. 48 (2009) 1082.
[18] P. Jia, X. Liu, Y. Luo, M. Yu, J. Lin, J. Electrochem. Soc. 154 (2007) J39.
[19] H. Meyssamy, K. Riwotzki, A. Kornowski, S. Naused, M. Haase, Adv. Mater. 11 (1999) 840.
[20] W.P. Zhang, P.B. Xie, C.K. Duan, K. Yan, M. Yin, L.R. Lou, S.D. Xia, J.C. Krupa, Chem. Phys. Lett. 292 (1998) 133.
[21] R.N. Bhargava, D. Gallaghar, X. Hong, A. Nurmikko, Phys. Rev. Lett. 72 (1994) 416.
[22] M. Yu, J. Lin, J. Fang, Chem. Mater. 17 (2005) 1783.
[23] M.G. Bawendi, W.L. Wilson, L. Rothberg, P.J. Carroll, T.M. Jedju, M.L. Steigerwald, L.E. Bruce, Phys. Rev. Lett. 65 (1990) 1623.
[24] A.P. Alivisatos, A.L. Harris, N.J. Lennos, S.L.E. Bruce, J. Chem. Phys. 89 (1988) 4001.
[25] K. Sharma Pramod, R. Nass, H. Schmidt, Opt. Mater. 10 (1998) 161.